NANO LETTERS

2007
Vol. 7, No. 9
2729−2733

Near-Static Dielectric Polarization of Individual Carbon Nanotubes

Wei Lu, Dan Wang, and Liwei Chen*

Department of Chemistry and Biochemistry, Ohio University, Athens, Ohio 45701

Received May 22, 2007; Revised Manuscript Received July 24, 2007

ABSTRACT

Low-frequency dielectric responses of carbon nanotubes are important for their manipulation, separation, and electronic applications. Here we report the first experimental measurement of near-dc polarization of individual carbon nanotubes by using modified scanning force microscopy techniques. The transverse polarizability of carbon nanotubes is equivalent to solid cylindrical media with a dielectric constant of about 10, irrespective of tube diameter and chirality. The longitudinal polarization is also observed and used to distinguish metallic from semiconducting nanotubes.

Single-walled carbon nanotubes (SWNTs) exhibit extraordinary mechanical, thermal, and electrical properties due to their unique one-dimensional all-carbon structure.[1] With the slightest twist in the structural chiral vector, SWNTs can be either metallic or semiconducting. The richness in structure and properties provides great opportunities in applications ranging from electronics, nanomedicine, composite materials, and alternative energy devices.[2−7] On the other hand, it also constitutes an enormous challenge to controllably synthesize, separate, and assemble nanotubes with desired properties in order to construct functional devices because as-synthesized SWNTs are always mixtures of a variety of tubes that include both metallic and semiconducting species.

Understanding the dielectric properties of SWNTs is critically important for their separation because the drastically different dielectric properties of metallic and semiconducting SWNTs are potentially the best basis for differentiation. Recent techniques such as ion-exchange chromatography[8,9] and dielectrophoresis[10,11] have started exploiting these differences for separation, but the mechanisms remain ambiguous and not fully resolved. In addition, dielectric properties can also be used to manipulate[12−14] and align[15−17] carbon nanotubes in electric fields, and they largely determine the screening effects in nanotube electronic devices and circuits.[18,19]

Despite the high level of attention on electronic transport and optical responses of SWNTs, the dc dielectric response has only been addressed sparsely and theoretically.[20−25] In general, the linear molecular polarizability matrix $\overleftrightarrow{A}$ of a SWNT is defined as

$$\vec{P}_{\text{in}} = \overleftrightarrow{A} \cdot \vec{E}_{\text{ex}} = \begin{pmatrix} \alpha_{xx} & \alpha_{xy} & \alpha_{xz} \\ \alpha_{yx} & \alpha_{yy} & \alpha_{yz} \\ \alpha_{zx} & \alpha_{zy} & \alpha_{zz} \end{pmatrix} \vec{E}_{\text{ex}}$$

where $\vec{E}_{\text{ex}}$ is the external field and $\vec{P}_{\text{in}}$ is the induced dipole moment of the SWNT. If $\hat{z}$ is the axial direction, and $\hat{x}$ and $\hat{y}$ are the radial directions, we have $\alpha_{xx} = \alpha_{yy} = \alpha_{\perp}$, the transverse polarizability, and $\alpha_{zz} = \alpha_{\parallel}$, the longitudinal polarizability. Tight-binding and density functional calculations agreed that, under the infinite length limit, the longitudinal polarization of truly metallic armchair carbon nanotubes is extremely large and does not converge in calculations.[20,23] Zigzag tubes, which include semiconducting tubes and semimetallic tubes with very small band gaps, show longitudinal polarizabilities proportional to the radius and inversely proportional to the square of the band gap. On the other hand, transverse polarizability of calculated armchair and zigzag nanotubes is proportional to the square of tube diameter but independent of tube chirality.[20,23] A recent study on the tight-binding level also provided insights on the finite length effects on the dielectric response of SWNTs as well as the intramolecular responses to impurities and perturbations.[26]

These works, however, have neither fully explored the tensorial nature of the polarizability nor correlated the calculated responses to the structural features of SWNTs. For example, the off-diagonal matrix elements of the molecular polarizability tensor of chiral nanotubes, which are expected to be nonzero, have not been calculated. More importantly, no experiments have been reported to check the validity of the theories. The difficulties of such experiments largely arise from the fact that nanotubes are highly anisotropic and most available nanotube samples are mixtures of species with vastly different dielectric properties.

* To whom correspondence should be addressed. E-mail: chenl1@ohio.edu.

10.1021/nl071208m CCC: $37.00
Published on Web 08/18/2007

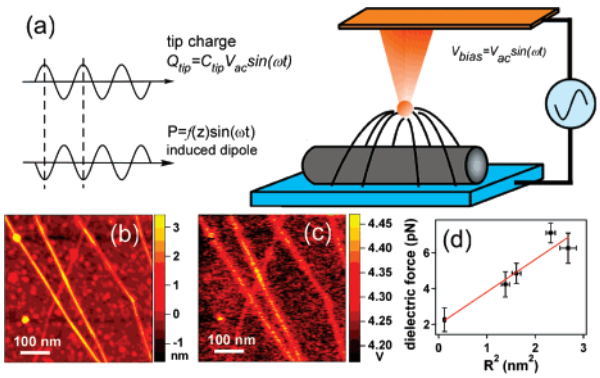

Figure 1. (a) Schematic illustration of the scanning force microscopy approach to the near-dc polarization of individual carbon nanotubes. (b) Topography and (c) dielectric images from a typical scan. (d) Quadratic dependence of the dielectric response on nanotube radius.

Here we report an experimental measurement of dielectric polarization of individual SWNTs as the first step toward understanding the carbon nanotube low-frequency dielectrics. A single-molecule approach using scanning force microscopy is adopted to overcome the heterogeneity in ensemble samples. Proximal force probes with nanometer spatial resolution are also capable of detecting forces as small as ~10 pN and thus are well-suited to measure the extremely small dielectric interaction forces from single carbon nanotubes.

Isolated SWNTs on degenerately p-doped Si wafer with a 2 nm thermal oxide layer were prepared via a chemical vapor deposition (CVD) process.[27] The Si substrate was cleaned in chloroform and blown dry under dry nitrogen gas and then dipped in freshly prepared $Fe(NO_3)_3 \cdot 9H_2O$ solution in isopropanol (0.1 mg/mL) for 20 s followed by rinsing in hexane. The iron nitrate coated substrate was heated at 800 °C in air, cooled down to 150 °C, and then run through the CVD program. First, the sample was heated up from 150 to 800 °C in 30 min under 600 sccm argon flow; second, 400 sccm of hydrogen gas was added for 15 min at 800 °C to reduce catalyst particles; finally, 31 sccm ethylene flow was supplied for 10 min at 800 °C for nanotube growth. The resulting sample had a density of about 5 tubes /μm^2 and the tube diameters range from 0.7 to 4.2 nm (Figure 1b). An Asylum Research MFP3D microscope (Santa Barbara, CA) was used to measure the nanotube polarization. The entire microscope was situated in a dry nitrogen (<1 ppm moisture) glove box (MBraun Inc., New Hampshire) to prevent moisture condensation and screening of the dielectric signal. Conducting atomic force microscope (AFM) tips with a resonance frequency about 60 kHz and spring constant of about 1.1 nN/nm were used in a double-pass imaging operation as previously published.[28] In the first pass, standard tapping mode imaging was performed to obtain the topography of a scan line (typical free resonance amplitude of 37.5 nm and amplitude set-point of 18 nm); a second pass of the same scan line then followed with the AFM tip lifted 18 nm above the topographical baseline and vibrating at 15 nm amplitude, while an oscillating bias potential $V = V_{dc} + V_{ac} \sin(\omega t)$ was applied between the tip and the Si substrate (ω = 500 Hz in all experiments). The bias field between the tip and the sample induces a polarization in carbon nanotubes. The induced dipole in turn interacts with the static charges on the conducting AFM tip and leads to an attractive force that oscillates in 2ω frequency (Figure 1a). The 2ω component of the AFM cantilever deflection signal, which is proportional to the force, was then sampled by a lock-in amplifier and recorded as the dielectric image.

Parts b and c of Figure 1 display topographical and dielectric images from a typical scan. The induced polarization of individual carbon nanotubes is clearly distinguishable on the background of the capacitive attraction force between the conducting AFM tip and the Si substrate. Figure 1d shows that the magnitude of the polarization has a quadratic dependence on the tube radius. Because the external field is predominantly perpendicular to the tube axis, and the interaction force is measured on the perpendicular direction, the tip−tube interaction is mostly dominated by the transverse polarization. Thus, the observed quadratic dependence agrees qualitatively with theoretical calculations that carbon nanotube transverse polarizability is proportional to the square of tube radius. A solid dielectric cylinder with radius R and isotropic dielectric constant ϵ would have transverse polarizability

$$\alpha_\perp = \frac{1}{2}\frac{\epsilon - 1}{\epsilon + 1} R^2$$

This suggests that the near-dc transverse dielectric response of carbon nanotubes can be approximated by solid cylindrical dielectric media with a uniform dielectric constant $\epsilon_\perp$ irrespective of tube diameter and chirality. Because the measurement geometry is well defined and the absolute force magnitude could also be obtained, we further the investigation in a quantitative manner to determine the transverse dielectric constant of carbon nanotubes and explore the influence of their longitudinal polarizability in nonuniform fields.

Crucial to the quantification of the dielectric force is the tip−substrate capacitance. The asymmetric pyramidal probe tip has been previously modeled as a conducting cone with a spherical apex.[28] The total capacitance is: $C_{total} = C_{sphere} + C_{cone} + C_{parellel-plate}$, in which C_{sphere}, C_{cone}, and $C_{parellel-plate}$ are the contributions from the sphere, the cone, and the cantilever beam, respectively. We calibrate the capacitance of each tip used in experiments by measuring the capacitive attractive force between the tip and the substrate

$$F = \frac{1}{2}\frac{dC_{total}}{dz} V^2$$

at different lift heights over an area with no carbon nanotubes or catalyst particles. The C_{total} is analytically expressed, and its derivative is used to fit the experimental data with a single fitting parameter, the radius of the sphere at the tip apex. Figure 2 shows capacitance calibration curves of two

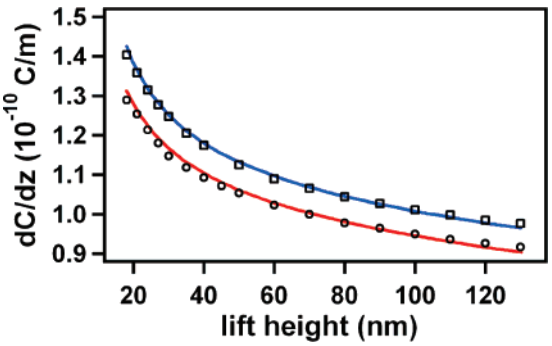

Figure 2. Capacitance calibration curve for two tips, open circles and squares are experimental data points; red and blue curves are the sphere−cone−parallel plate fit for the two tips with a single fitting parameter: tip radius being 12 and 14 nm, respectively.

different tips with fitting. Tip sphere radii of about 10−15 nm are typically observed, which are in good agreement with vendor specification and previous calibration using frequency shift detection.[28]

The determination of the tip−substrate capacitance and the tip sphere radius allows us to build an electrostatic model including carbon nanotubes. The presence of pseudo-one-dimensional nanotubes breaks the symmetry of the system and thus the model can only be solved numerically. A finite-element analysis package (Multiphysics 3.3, COMSOL, Inc., Burlington, MA) is used to solve the Poisson's equation in a cylindrical space that includes the tip represented by a metallic cone combined with a hemisphere ($\epsilon = 10\,000$) whose radius is determined from tip-capacitance calibration, 2 nm SiO_2 layer ($\epsilon = 3.9$), and the carbon nanotube represented by a solid cylindrical media whose dielectric characteristics are to be tried and compared with experiments. The boundary condition is that the potential is 5 V at the tip surface and 0 V at the bottom surface of the SiO_2 layer; the electric displacement, $\vec{D} = \epsilon\epsilon_0\vec{E}$, is required to be continuous across all other surfaces and interfaces at their normal directions. The attractive force exerted on the tip is calculated as

$$F = \oint_{\text{tip-surface}} \frac{1}{2}\,\vec{D}\cdot\vec{E}\cdot\mathrm{d}s$$

In this model, the $C_{\text{parallel-plate}}$ contribution from the cantilever beam is neglected because the distance between the substrate and the plate ($>10\ \mu$m) is much greater than any variations of the height that may be encountered in the nanotube measurements. The length of the nanotube and the spatial dimension of the field to be included in the model are determined from multiple trials to minimize the finite size effect and maximize the calculation efficiency.

Figure 3 shows the cross-section view of a solved electrostatic potential distribution. When the dielectric constant of the nanotube cylinder is set to 1, the attractive force on the tip calculated from the numerical model reduces to that of the sphere and cone model for the tip capacitance. Figure 4 compares experimental results with numerically modeled forces using an isotropic dielectric cylinder model

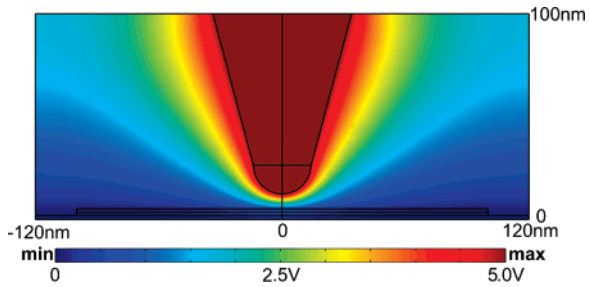

Figure 3. Cross-section of a numerically solved potential distribution at the vicinity of the tip and carbon nanotube. The model encloses a cylindrical space of 120 nm in radius and 100 nm in height. The tip radius: 14 nm; tip cone angle: 15°; nanotube length: 200 nm. A total of about 500 000 finite elements were defined with mesh size of 0.4 and 2 nm on nanotube and tip surfaces, respectively.

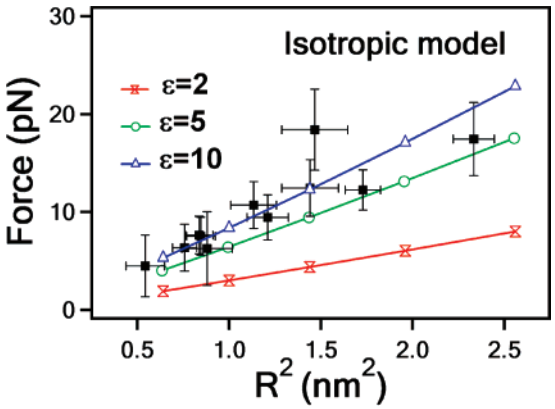

Figure 4. Comparison between measured dielectric forces of carbon nanotubes and those obtained from numerical calculations using isotropic models. The error bars are the standard deviation of signals measured from multiple pixels along the tube axis.

for carbon nanotubes. Both the experimental and numerical results recover the R^2 dependence observed in theoretical calculation and qualitative imaging. Moreover, the experimental measurements can be well fit with an isotropic dielectric constant of about 10, suggesting the simplified model of an isotropic dielectric cylinder catches essential features of the dielectric responses in the predominantly transverse configuration of the measurement.

The longitudinal dielectric properties differentiate metallic and semiconducting nanotubes. Interestingly, we observe the influence of longitudinal polarization in both the numerical modeling and the experiments. Parts a and b of Figure 5 display numerically calculated potential distributions around a metallic and a semiconducting carbon nanotube, whose longitudinal dielectric constants are approximately set to 1000 and 30, respectively.[23] The transverse dielectric constant for both tubes is set to 10. In the metallic model ($\epsilon_{||} = 1000$), the high $\epsilon_{||}$ screens the external field effectively and forms equal potential surfaces parallel to the axis (Figure 5a). In the semiconducting model ($\epsilon_{||} = 30$), screening of the external field is less effective and localized bound charges accumulate mostly below the tip (Figure 5b). Consequently, the potential difference between the tip and the nanotube is larger in metallic tubes, which results in stronger attraction between the tip and a metallic tube.

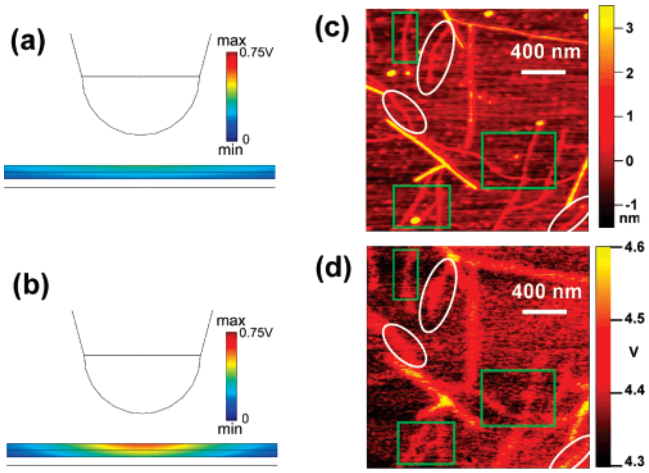

Figure 5. Influence of the longitudinal polarizability. Potential distributions around (a) a metallic nanotube and (b) a semiconducting nanotube show significant differences, which result in stronger interaction forces between the probe tip and metallic tubes than semiconducting tubes. Topographical (c) and dielectric (d) images of nanotubes: tubes in white open ovals are metallic and those in green open squares are semiconducting.

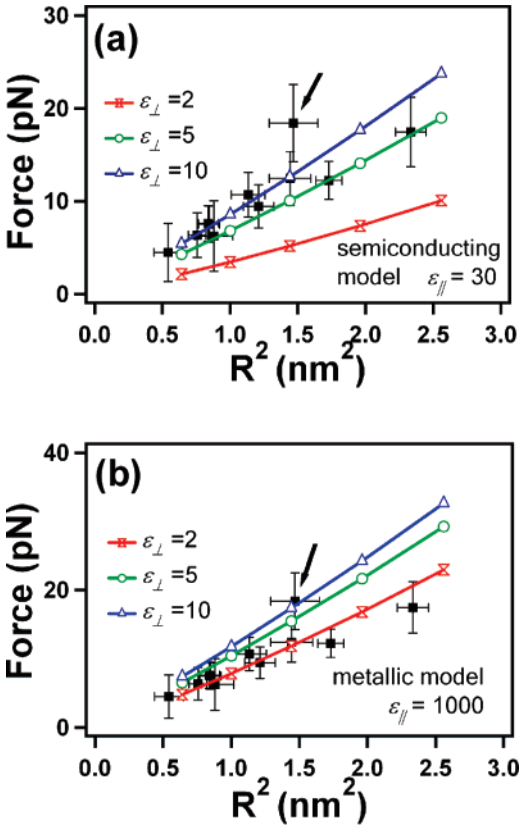

Figure 6. Comparison between measured dielectric forces and those from anisotropic metallic and semiconducting models. The error bars are the standard deviation of signals measured from multiple pixels along the tube axis.

This effect could be used to distinguish metallic from semiconducting carbon nanotubes. Parts c and d of Figure 5 show the topographical and dielectric images of a scan area with multiple SWNTs. The tubes encircled in open white ovals have diameters comparable to those in green open squares (Figure 5c) but display much greater polarizability, as seen in the dielectric image (Figure 5d). Figure 6 compares experimental data with numerical results by using anisotropic dielectric models. The semiconducting model ($\epsilon_{||} = 30$) with $\epsilon_\perp$ between 5 and 10 agree well with most of experimental data points except for one (black arrow), which would require an unrealistically high $\epsilon_\perp$ of 2000 in the semiconducting model to match the measured dielectric force (Figure 6a). On the other hand, a metallic model ($\epsilon_{||} = 1000$) with $\epsilon_\perp = 10$ fits this tube well but would lead to $\epsilon_\perp < 2$ for many other tubes (Figure 6b). We thus conclude that this tube is metallic, while other tubes are semiconducting. A transverse dielectric constant $\epsilon_\perp \sim 10$ fits well for both metallic and semiconducting tubes. This yields a coefficient $C \sim 0.41$ in transverse polarizability

$$\alpha_\perp = \frac{1}{2}\frac{\epsilon_\perp - 1}{\epsilon_\perp + 1} R^2 = CR^2$$

which is consistent with the theoretical prediction of $C = 0.40$.

In summary, we report the first experimental measurement of the near-dc polarization of individual carbon nanotubes. We conclude that the transverse dielectric response can be approximated by solid cylindrical media with a dielectric constant of about 10, irrespective of the tube diameter and chirality. The nonuniform field around the scanning local probe also results in a weak but discernible influence from the longitudinal polarization, which could be used to distinguish metallic from semiconducting nanotubes. Further optimization of the measurement geometry could potentially lead to better determination of the transverse and longitudinal polarizabilities, and even identify the off-diagonal elements in the polarizability matrix. The experiment establishes a general method for investigating dielectric properties of inhomogeneous and anisotropic nanomaterials.

Acknowledgment. We thank Sergio Ulloa and Nicola Marzari for valuable discussions. This work is partially supported by Ohio University Research Council and Ohio University Biomimetic Nanoscience and NanoTechnology program.

References

(1) R. Saito, G. D.; Dresselhaus, M. S. *Physical Properties of Carbon Nanotubes*; Imperial College Press: London, 1998.
(2) Avouris, P. *Acc. Chem. Res.* **2002**, *35*, 1026−1034.
(3) Baughman, R. H.; Zakhidov, A. A.; de Heer, W. A. *Science* **2002**, *297*, 787−792.
(4) Cherukuri, P.; Gannon, C. J.; Leeuw, T. K.; Schmidt, H. K.; Smalley, R. E.; Curley, S. A.; Weisman, R. B. *Proc. Natl. Acad. Sci. U.S.A.* **2006**, *103*, 18882−18886.
(5) Kam, N. W. S.; O'Connell, M.; Wisdom, J. A.; Dai, H. J. *Proc. Natl. Acad. Sci. U.S.A.* **2005**, *102*, 11600−11605.
(6) Guldi, D. M. *J. Phys. Chem. B* **2005**, *109*, 11432−11441.
(7) Guldi, D. M.; Rahman, G. M. A.; Zerbetto, F.; Prato, M. *Acc. Chem. Res.* **2005**, *38*, 871−878.
(8) Zheng, M.; Jagota, A.; Semke, E. D.; Diner, B. A.; McLean, R. S.; Lustig, S. R.; Richardson, R. E.; Tassi, N. G. *Nat. Mater.* **2003**, *2*, 338−342.
(9) Zheng, M.; Jagota, A.; Strano, M. S.; Santos, A. P.; Barone, P.; Chou, S. G.; Diner, B. A.; Dresselhaus, M. S.; McLean, R. S.; Onoa, G. B.; Samsonidze, G. G.; Semke, E. D.; Usrey, M.; Walls, D. J. *Science* **2003**, *302*, 1545−1548.

(10) Krupke, R.; Hennrich, F.; von Lohneysen, H.; Kappes, M. M. *Science* **2003**, *301*, 344−347.
(11) Peng, H.; Alvarez, N. T.; Kittrell, C.; Hauge, R. H.; Schmidt, H. K. *J. Am. Chem. Soc.* **2006**, *128*, 8396−8397.
(12) Krupke, R.; Hennrich, F.; Weber, H. B.; Kappes, M. M.; von Lohneysen, H. *Nano Lett.* **2003**, *3*, 1019−1023.
(13) Tang, J.; Yang, G.; Zhang, Q.; Parhat, A.; Maynor, B.; Liu, J.; Qin, L. C.; Zhou, O. *Nano Lett.* **2005**, *5*, 11−14.
(14) Li, J. Q.; Zhang, Q.; Peng, N.; Zhu, Q. *Appl. Phys. Lett.* **2005**, *86*, 153116.
(15) Joselevich, E.; Lieber, C. M. *Nano Lett.* **2002**, *2*, 1137−1141.
(16) Ural, A.; Li, Y. M.; Dai, H. J. *Appl. Phys. Lett.* **2002**, *81*, 3464−3466.
(17) Zhang, Y. G.; Chang, A. L.; Cao, J.; Wang, Q.; Kim, W.; Li, Y. M.; Morris, N.; Yenilmez, E.; Kong, J.; Dai, H. J. *Appl. Phys. Lett.* **2001**, *79*, 3155−3157.
(18) Li, Y.; Rotkin, S. V.; Ravaioli, U. *Nano Lett.* **2003**, *3*, 183−187.
(19) Lin, M. F.; Chuu, D. S. *Phys, Rev, B* **1997**, *56*, 4996−5002.
(20) Benedict, L. X.; Louie, S. G.; Cohen, M. L. *Phys. Rev. B* **1995**, *52*, 8541−8549.
(21) Jensen, L.; Schmidt, O. H.; Mikkelsen, K. V.; Astrand, P. O. *J. Phys. Chem. B* **2000**, *104*, 10462−10466.
(22) Leonard, F.; Tersoff, J. *Appl. Phys. Lett.* **2002**, *81*, 4835−4837.
(23) Kozinsky, B.; Marzari, N. *Phys. Rev. Lett.* **2006**, *96*, 166801.
(24) Novikov, D. S.; Levitov, L. S. *Phys. Rev. Lett.* **2006**, *96*, 036402.
(25) Brothers, E. N.; Kudin, K. N.; Scuseria, G. E.; Bauschlicher, C. W. *Phys. Rev. B* **2005**, *72*, 033402.
(26) Lu, D. Y.; Li, Y.; Rotkin, S. V.; Ravaioli, U.; Schulten, K. *Nano Lett.* **2004**, *4*, 2383−2387.
(27) Cheung, C. L.; Kurtz, A.; Park, H.; Lieber, C. M. *J. Phys. Chem. B* **2002**, *106*, 2429−2433.
(28) Cherniavskaya, O.; Chen, L. W.; Weng, V.; Yuditsky, L.; Brus, L. E. *J. Phys. Chem. B* **2003**, *107*, 1525−1531.

NL071208M